Title: Enhanced protein synthesis is a defining requirement for neonatal B cell development

Running title: Early-life B cell output depends on enhanced protein synthesis

Hugo Åkerstrand*, Elena Boldrin*, Giorgia Montano*, Stijn Vanhee*, Karin Olsson*, Niklas Krausse*, Stefano Vergani*, Maciej Cieśla†, Cristian Bellodi†, Joan Yuan*

* Developmental Immunology Unit, Department of Molecular Hematology, Lund Stem Cell Center, Lund University, Lund, Sweden

† RNA and Stem Cell Biology Unit, Department of Molecular Hematology, Lund Stem Cell Center, Lund University, Lund, Sweden

Corresponding author: +46462220430, joan.yuan@med.lu.se

Abstract

Protein synthesis is a stringently regulated process that fundamentally dictates capacity for cellular growth. Rapid fluctuations in cell size and proliferation characterize B cell development. However, little is known about how ribosomal control may impact this process. Here, we identify elevated protein synthesis as a defining feature of early-life B cell development and a determinant for the output of self-reactive CD5+ B-1 cells in mice. Interactome analyses in primary B cell precursors showed direct binding of the heterochronic RNA binding protein LIN28B to ribosomal protein transcripts, which correlated with their elevated protein expression *in vivo*. Genetic perturbations demonstrated that LIN28B is both necessary and sufficient to elevate protein synthesis during the small Pre-B and immature B cell stages. Interestingly, IL-7 signaling was the dominant driver of the c-MYC/ribosome axis in earlier stages and masked LIN28B induced protein synthesis in Pro-B cells. Finally, we demonstrated that subdued protein synthesis was detrimental for neonatal B cell development and the output of self-reactive B-1 cells, without affecting the adult. Thus, LIN28B elevates ribosomal capacity to shape the naïve B cell repertoire in neonatal life.

Introduction

B-cell development is centered around alternating stages of cellular proliferation and V(D)J recombination at the immunoglobulin heavy and light chain loci, with the goal of producing a diverse yet self-tolerant B cell repertoire. During the Pro-B cell stage, productive IgH rearrangement results in the expression of a pre-BCR complex and differentiation into the large Pre-B cell stage. The latter is marked by a transient burst of clonal expansion. Cell cycle exit is accompanied by the initiation of light chain recombination and entry into the small Pre-B cell stage. IL-7 signaling is an essential trophic factor during the Pro- and large Pre-B cell stages, promoting cell survival, proliferation, and differentiation, through distinct effects mediated by the Stat5 and mTORC1/c-MYC signaling axes (1, 2). IL-7 signaling wanes as large Pre-B cells move away from IL-7 producing stromal cells in vivo and its attenuation is required for the developmental progression into the small Pre-B cell stage and the onset of IgK light chain recombination (3). Generation of a productive immunoglobulin heavy and light chain complex leads to membrane IgM expression and developmental progression into the immature B (Imm-B) cell stage. Here, cells carrying innocuous BCRs are allowed to mature while self-reactive specificities are subject to central tolerance mechanisms including receptor editing and apoptosis to remove potentially harmful recognition of “self” (4). Progression through these stages is accompanied by dramatic fluctuations in bioenergetic states. Although metabolic capacity has been proposed to modulate the central tolerance checkpoint (5), this theory has not been empirically proven.

Much of what we know about B cell development comes from studies in adult mice, which differs significantly from fetal and neonatal life. For example, while B cell development in adult bone marrow strictly requires IL-7 mediated signaling, B cell output can take place in neonatal mice lacking IL-7Ra until around two weeks of age (6). Furthermore, both the pre-

53 BCR and mature BCR checkpoints are less stringent during neonatal life allowing for the
54 positive selection of poly and self-reactive specificities in mice and men (7-9). This correlates
55 with the output of CD5+ B-1 cells in mice, which secrete natural antibodies important for the
56 clearance of cellular debris and act as a first line of defense against pathogens (10). Despite
57 these differences, the basis for the developmental switch in B cell output is not well understood.
58
59 One molecular program that distinguishes early life lymphopoiesis is centered around the post-
60 transcriptional regulator LIN28B. It is one of two mammalian homologs of *lin-28* first
61 identified in *Caenorhabditis elegans* to encode a heterochronic RNA binding protein in control
62 of the timing of larval development (11). In the mammalian hematopoietic system, *Lin28b*
63 expression is abundant during fetal life and gradually silenced within the first two to three
64 weeks of life, critically controlling a neonatal switch in hematopoietic stem cell function and
65 lineage output patterns (12). Like its mammalian paralog *Lin28a*, *Lin28b* plays an established
66 role in regulating organismal growth and cellular metabolism, most famously through the direct
67 inhibition of the biogenesis of the evolutionarily conserved Let-7 family of microRNAs.
68 LIN28A/B expression de-represses Let-7 targets which include the proto-oncogenes *Myc*,
69 *Arid3a*, *Hmga2* and *Igf2bp1-3* (13-15). We and others have previously shown that ectopic
70 LIN28A/B expression in the adult promotes key aspects of fetal-like lymphopoiesis, including
71 the efficient production of CD5+ B-1 cells (13, 16-18). Furthermore, studies from both BCR
72 poly-clonal and transgenic mouse models make clear that LIN28B relaxes the central tolerance
73 checkpoint to allow for the positive selection of self-reactive BCR specificities and thereby
74 uniquely shapes the neonatal B cell repertoire (19, 20). The mechanism for this effect is,
75 although not fully understood, at least in part linked to augmentation of c-MYC protein levels
76 in Imm-B cells and the CD19/PI3K/c-MYC positive feedback loop (19) known to promote B
77 cell positive selection (21).

78

79 A less understood mechanism of LIN28B action is through the direct binding of coding
80 mRNAs to either positively or negatively regulate transcript stability and protein translation,
81 in a context dependent manner (22-31). In particular, several studies have demonstrated the
82 ability of LIN28B to promote the translation of ribosomal proteins, through Let-7 independent
83 direct binding to their transcripts in human ES cells (32), transformed human kidney (22) and
84 neuroblastoma (31) cell lines. However, the role of the protein synthesis pathway in LIN28B
85 dependent B cell positive selection is not known. Here we demonstrate that LIN28B directly
86 interacts with ribosomal protein transcripts in primary B cell precursors. Importantly, LIN28B
87 expression is necessary and sufficient to elevate protein synthesis specifically during the later
88 stages of IL-7 independent bone marrow B cell maturation. Finally, we show that an augmented
89 mode of protein synthesis is a hallmark of neonatal B cell development and a pre-requisite for
90 the positive selection of self-reactive Imm-B cells and the output of CD5+ B-1 cells early in
91 life. We propose that the post-transcriptional actions of LIN28B cooperates with the
92 transcriptional regulation of ribosomal components by c-MYC to augment protein synthesis
93 and support neonatal B lymphopoiesis.

Materials and methods

Mice

tet-LIN28B mice were generated by intercrossing *Col1a*$^{tetO\text{-}LIN28B}$ (The Jackson Laboratory, #023911) to *Rosa26*^{rtTA*m2} (The Jackson Laboratory, #006965) mice and were originally obtained from the laboratory of George Daley (Harvard Medical School) (33). Transheterozygous mice were used for experiments. *Rosa26*^{rtTA*m2} heterozygous littermates were used as control mice. Doxycycline chow (200 mg/kg, Ssnif, cat#A112D70203) was fed to tet-LIN28B and littermates for 10 days before analysis. B6.Cg-*Lin28b*$^{tm1.1Gqda}$/J (*Lin28b* KO) (The Jackson Laboratory, #023917) and C57BLKS-*Rpl24*^{Bst}/J (Bst) (The Jackson Laboratory, #000516) were originally purchased from the Jackson laboratory. Wildtype mice were originally purchased from Taconic (B6NTAC, Taconic). The *Lin28b*-eGFP knock-in strain was generated as previously described (34). Adult mice were used at 10 to 16 weeks of age, neonates were analyzed at the indicated days post-birth. Male and female mice were used interchangeably throughout the experiments. Animal husbandry and experimental procedures were performed in accordance with ethical permits issued by the Swedish Board of Agriculture.

Bone marrow cultures

Adult bone marrow B cell precursors were expanded and enriched *ex vivo*, as previously described (35). Briefly, single cell suspension of red blood cell lysed bone marrow was plated in pre-warmed RPMI-1640 (Fischer Scientific, cat#21875091) and incubated for 15 min at 37 ºC. The non-adherent cells were isolated and seeded at a cell density of 0.75-1.5 million/mL using fully supplemented RPMI-1640, IL-7 (20 ng/mL, Peprotech, cat#217-17), and doxycycline (0.1 µg/ml, Sigma-Aldrich, cat#D3072). The cell culture medium was refreshed every second day.

119 **RNA Immunoprecipitation Sequencing (RIP-seq)**

120 Cells from day 5 bone marrow cultures from tet-LIN28B or littermate control mice were used
121 for lysis and RIP using Magna RIP RNA-Binding Protein Immunoprecipitation kit (Millipore,
122 cat#17-700) according to the manufacturer's instructions. Briefly, 10% of the total lysate was
123 kept as input sample. 4 µg of anti-Flag antibody (Sigma) and 50 µl of A/G beads (Millipore,
124 cat#16-663) were added to the lysate and incubated for 3 hours. Beads were washed 6 times
125 with ice-cold RIP wash buffer (Millipore, cat#17-700). RNA was extracted using RNAzol
126 (Sigma-Aldrich, cat#R4533) and Direct-zol RNA MicroPrep kit (Zymo Research, cat#R2060).
127 For RNA quantification and quality control respectively, Qubit with RNA HS kit
128 (Thermofisher Scientific, cat# Q32852) and Agilent Bioanalyzer with RNA Pico kit (Agilent,
129 cat#5067-1513) were used according to the manufacturer's instructions. 20ng of total RNA
130 was used for the cDNA synthesis and amplification with the SMART-Seq v4 Ultra Low Input
131 RNA Kit for Sequencing (Takara, cat#634889) according to instructions. Library tagmentation
132 and indexing was performed using Nextera XT DNA Kit (Illumina, cat#FC-121-1030) and
133 Nextera XT v2 set A Indexing kit (Illumina, cat#15052163). Library quantification and library
134 size were measured using Qubit DNA HS kit (Thermofisher Scientific, cat#Q32851) and
135 BioAnalyzer DNA HS kit (Agilent, cat#5067-4626). The samples were run in NextSeq 550
136 using NextSeq High output 150 cycles 2x76bp. Reads were aligned using STAR aligner v2.7.1
137 to mm10 and counted using RSEM v1.28. Genes were filtered for an FPKM of at least 50 in
138 total tet-LIN28B input samples and following LIN28B immunoprecipitation. Enrichment was
139 calculated as IP over Input FPKM for each of the two tet-LIN28B samples individually. 238
140 transcripts had an average enrichment of at least 2-fold and were considered for subsequent
141 analyses. Littermate control sample was not considered when generating this list. Gene
142 ontology analysis was done using the Panther database (pantherdb.org, release 17.0). Data is
143 accessible through (GEO number, data is submitted and being processed).

144

145 **RNA sequencing**

146 RNA sequencing was performed on sorted adult bone marrow large Pro-B, large Pre-B, small
147 Pre-B, or Imm-B cell subsets. Data is accessible through (GEO number, data is submitted and
148 being processed) except for Imm-B that was previously generated (19) and is accessible
149 through GSE135603. All data was processed and analyzed as previously described (19). GSEA
150 used Wald's stat as ranking metric.

151

152 **Metabolic labeling of nascent proteins**

153 Cells were depleted of endogenous methionine by pre-culturing them in methionine free RPMI
154 (Fisher Scientific, cat#A1451701). After 45 minutes, the medium was supplemented with L-
155 azidhomoalanine (AHA, 1 mM final concentration, Fisher Scientific, cat#C10102) and labeled
156 for one hour. AHA uptake was visualized using Click-iT Plus Alexa Fluor 555 Picolyl Azide
157 Toolkit (Fisher Scientific, cat#C10642), following the manufacturer's protocol. Briefly, up to
158 3 x 10^6 cells were fixed in 400 µL of 4% formaldehyde (Fischer Scientific, cat#28906) for 20
159 minutes at room temperature, washed, and then permeabilized in equal amounts of 0.1%
160 saponin (Sigma, cat#S4521) for 20 minutes. Alexa Fluor 488 Alkyne (Fisher Scientific,
161 cat#A10267) was used in place of Alexa Fluor 555 for FACS analysis.

162

163 **Flow cytometry**

164 Bone marrow cells were extracted by crushing bones from hind- and front limbs, hips, and
165 sternum, using mortar and pestle. Peritoneal cavity was isolated by flushing adult mice with 8
166 mL of FACS buffer (Hank's Balanced Salt Solution (Gibco, cat#14175-053) supplemented
167 with 0.5% Bovine Serum Albumin (Sigma, cat#A9647) and 2 mM EDTA (Invitrogen,
168 cat#15575-038)), or neonates 1-2 mL depending on the age. Red blood cell lysis was performed

169 on bone marrow and spleens using ACK lysis buffer (Fischer Scientific, cat#A1049201), only
170 for mice that were at least 19 days old. Lineage depletion was carried out before cell sorting by
171 MACS Cell Separation and LS columns (Miltenyi Biotec, cat#130-042-401) to deplete CD3+,
172 TER119+, or Gr-1+ cells, according to manufacturer's instructions.
173
174 Antibody staining of surface antigen was performed using FACS buffer, at a cell density of 1
175 x 10^7 cells per 100 µL of FACS buffer with antibodies, for 30 minutes at 4 ºC. Analysis of
176 intracellular antigens was done by using BD Cytofix/Cytoperm fixation/permeabilization kit
177 (BD Biosciences, cat#554714), using a maximum of 3 x 10^6 cells per reaction. All flow
178 cytometry experiments were gated on live CD19+ B cells and the following
179 immunophenotypes: Pro-B cells (CD93+IGM–cKIT+), Pre-B cells (CD93+IGM–cKIT– and
180 FSC-A to separate large from small), Imm-B cells (CD93+IGM+), peritoneal cavity B-1a B
181 cells (CD5+CD23–B220low and CD43+), and peritoneal cavity B-2 B cells (B220high CD23+
182 and CD43–). All flow cytometry experiments were performed at the Lund Stem Cell Center
183 FACS Core Facility (Lund University) using BD Fortessa, BD Fortessa X20, BD FACS Aria
184 III, or BD FACS Aria II instruments. Cell sorting was performed using a 70 µm nozzle, 0.32.0
185 precision mask, and a flow rate below 6000 events/s. Analysis was performed using FlowJo
186 version 10. Antibodies are listed in Supplemental table S1.
187
188 **In vivo treatment with Rapamycin**
189 Rapamycin (Enzo LifeSciences, cat#BML-A275-0005) was dissolved in Ethanol (99.5%,
190 Solveco, cat#11594139) and stocked at a concentration of 10 mg/mL. Further dilution was
191 done in sterile DPBS (Cytiva, cat#SH30028.02) before administering a single intraperitoneal
192 injection of Rapamycin (2.5 mg/kg) or vehicle control (36).
193

194 **Western Blot**

195 Sorted B cells were lysed in RIPA buffer (CST, cat#9806S), protease inhibitor (Roche,
196 cat#4693132001), and PMSF (CST, cat#8553S). Loading samples were prepared with
197 Laemmli buffer (Bio-Rad, cat#1610747) with β-mercaptoethanol (Bio-Rad, cat#1610710).
198 Proteins were separated by SDS–polyacrylamide gel electrophoresis (Any kD Mini-Protean
199 TGX gel, Bio-Rad, cat#4568125) and transferred to a nitrocellulose membrane (Trans-Blot
200 Turbo Mini Nitrocellulose Transfer Packs, Bio-Rad, cat#1704158). Membranes were blocked
201 for 1 hour at RT in 5% skimmed milk. Antibodies are listed in Supplemental table S2. The
202 ECL Select kit (GE Healthcare, cat#RPN2235) was used to detect protein bands with a
203 ChemiDoc XRS+ system (Bio-Rad).

204

205 For RIP validation western blot of Pro-B cells cultured ex vivo from bone marrow, 10% of the
206 total protein extract was collected to validate the immunoprecipitation efficiency. Proteins were
207 separated by SDS–polyacrylamide gel electrophoresis (12% Mini-Protean TGX gel, Bio-Rad,
208 cat#4561043) and transferred to a nitrocellulose membrane (Trans-Blot Turbo Mini
209 Nitrocellulose Transfer Packs, Bio-Rad, cat#1704158). Membranes were blocked for 1 hour at
210 RT in 5% skimmed milk. Antibodies are listed in Supplemental table S2.

211

212 **qRT-PCR**

213 50.000 sorted cells were lysed in RNAzol (Sigma-Aldrich, cat#R4533) and total RNA was
214 extracted using Direct-zol RNA MicroPrep kit (Zymo Research, cat#R2060) according to the
215 manufacturer's instructions. Total RNA (8 µl) was used in random primed cDNA synthesis
216 with TaqMan Reverse Transcription Reagents (Applied Biosystem, cat#N8080234). Diluted
217 cDNA 1:2 (4 µl) was used in every qPCR reaction using KAPA probe Fast qPCR kit (Kapa
218 Biosystem, cat#KK4706) with primers targeting 45S (Thermofisher Scientific, cat#

219 Mm03985792_s1) and 18S (Thermofisher Scientific, cat# 4333760T) rRNA transcripts. The
220 relative expression levels of rRNA were evaluated using log2 (2ΔCt) calculation.
221
222 **Statistical analysis**
223 All statistical analysis was carried out in R (version 4.1.2) and RStudio (version 1.4.1717),
224 using functions from the following packages: tidyverse (version 1.3.1), DESeq2 (version
225 1.32.0), rstatix (version 0.7.0), and ggpubr (version 0.4.0).
226
227 **Antibodies**
228 Antibodies are listed in Supplemental table 1 (Flow cytometry) and 2 (Western blot and
229 Immunoprecipitation).

230 **Results**

231

232 **The LIN28B mRNA interactome in primary B cell precursors is enriched for ribosomal**
233 **protein transcripts**

234 To identify direct mRNA targets of LIN28B that could be important during normal B cell
235 development, we took advantage of tet-LIN28B mice which express ectopic FLAG tagged
236 human LIN28B upon doxycycline (Dox) treatment (33). To obtain sufficient cell numbers, B
237 cell precursors from tet-LIN28B and control mice were expanded for 5 days *ex vivo* from whole
238 bone marrow cultures in the presence of IL-7 and Dox (Supplemental figure 1A). Cultured
239 cells were subsequently subjected to RNA co-immunoprecipitation (IP) coupled with poly-A
240 selected RNA-sequencing (RIP-seq) (Figure 1A). Immunoprecipitation efficiency of LIN28B
241 was validated by western blot analysis (Supplemental figure 1B). Total RNA sequencing of
242 corresponding input samples was used for calculating RIP-seq enrichment. RIP/input ratio of
243 the technical replicates showed a high degree of correlation ($R=0.93$, $p < 2.2e-16$) (Figure 1B)
244 and were averaged for downstream analyses. 238 transcripts displayed a higher than two-fold
245 RIP/input enrichment in tet-LIN28B samples but showed no trend in the control (Supplemental
246 Table 3 and Figure 1C). Gene ontology (GO) analysis revealed a prominent enrichment for
247 ribosomal protein coding transcripts (Figure 1D), suggesting that ribosomal function might be
248 a core target pathway of LIN28B during B cell development. Interestingly, similar observations
249 were previously made in other cell types, including 293T cells (22) and BE(2)-C neuroblastoma
250 cells (31). Indeed, cross comparison of our identified targets with these studies yielded
251 cytoplasmatic translation as the predominant overlapping GO term (Figure 1E-F). Our analysis
252 also identified other GO terms involved in RNA splicing and oxidative phosphorylation,
253 consistent with previous LIN28A/B interactome studies in various cell types (23, 37). We
254 conclude that the direct LIN28B mRNA regulon in the context of primary bone marrow B cell

255 progenitor cells is dominated by transcripts implicated in universal biosynthetic pathways,
256 which are shared across a wide range of cell types. In particular, our findings implicate the
257 ribosome as a potential target for LIN28B regulation in B cell progenitors.
258

259 **LIN28B enhances protein synthesis in the later stages of B cell development**

260 LIN28B bound mRNA targets have been linked to both translational increase and decrease in
261 a context dependent manner (22-31). In the case of ribosomal protein transcripts, enhanced
262 protein translation was shown by stable isotope labeling using amino acid in culture (SILAC)
263 (22) and polysome profiling (31). To assess ribosomal protein levels during B cell
264 development, we performed western blot analysis on 50,000 sorted B cell precursors from tet-
265 LIN28B and control mice following 10 days of Dox induction *in vivo* (Supplemental figure
266 2A). As expected, based on the dynamic changes in bioenergetic states during B cell
267 development, the expression of ribosomal proteins rise and fall in the large and small Pre-B
268 cell stages, respectively (Figure 2A). Consistent with enhanced translation, we found increased
269 levels of ribosomal proteins upon LIN28B induction throughout B cell development.
270

271 Given the increase in ribosomal proteins, we expected a corresponding increase in ribosomal
272 RNA (rRNA) content. To this end, we measured the 18S rRNAs by qRT-PCR of FACS sorted
273 B cell precursors. To our surprise, we detected no LIN28B dependent differences in Pro-B or
274 large Pre-B cells. Instead, rRNA content first began to increase in a LIN28B dependent manner
275 in the small Pre-B cell stage reaching statistical significance in Imm-B cells (Figure 2B).
276 Additional analysis of the 45S precursor rRNA followed the same trend (Figure 2C). Thus,
277 increased ribosomal protein levels precede increased ribosome biogenesis during LIN28B
278 induced B cell development *in vivo*. To evaluate whether this observation correlates with
279 changes in global protein synthesis rates we measured newly synthesized proteins in freshly

280 isolated B cell precursors using metabolic labelling with the methionine analog L-
281 azidohomoalanine (AHA) (38). As expected, FACS readout of AHA uptake from Dox induced
282 control and tet-LIN28B mice showed highly dynamic protein synthesis levels during B cell
283 development (Figure 2D). Pro-B cells exhibited a bimodal profile with respect to protein
284 synthesis that correlated with cell size (AHA^{high} or AHA^{low}, Supplemental figure 2B). Although
285 there was a slight tendency towards more AHA^{high} Pro-B cells in tet-LIN28B induced mice, no
286 statistical significance was detected in either the median fluorescence intensity or frequency of
287 the two subsets (Figure 2E, Supplemental figure 2C). Instead, LIN28B induced a progressive
288 increase in global protein synthesis after the Pro-B cell stage, peaking in Imm-B cells. Protein
289 synthesis in mature B-1 and B-2 cells were not affected by LIN28B expression (Figure 2F).
290 Taken together, we conclude that LIN28B enhances ribosome content and global protein
291 synthesis levels during the later stages of bone marrow B cell development.
292

293 **IL-7 responsiveness dictates the stage specific effects of LIN28B during B cell**
294 **development**

295 Elevated ribosomal biogenesis is a hallmark of c-MYC activity (39). We have previously
296 shown that LIN28B upregulates c-MYC protein expression in Imm-B cells (19). However, the
297 status of LIN28B induced c-MYC in earlier B cell precursor stages is not known. Given our
298 insight on ribosomal content and protein synthesis, we analyzed c-MYC protein levels
299 throughout B cell development using intracellular FACS. Consistent with its known IL-7
300 driven expression in Pro-B cells (2, 40), we found that c-MYC peaked in a subset of Pro-B
301 cells regardless of genotype. The impact of LIN28B on c-MYC expression began after the Pro-
302 B cell stage and culminated in Imm-B cells (Figure 3A-B), mirroring the trend observed for
303 protein synthesis. These findings are also observed at the transcriptome level, where gene set
304 enrichment analysis (GSEA) identified a LIN28B induced c-MYC target gene signature

305 succeeding the IL-7 dependent Pro-B and large Pre-B stages (Figure 3C). The same trend was
306 observed for LIN28B RIP-seq targets, consistent with c-MYC driving ribosome biogenesis. In
307 contrast, LIN28B induced de-repression of Let-7 targets was most prominent during the IL-7
308 dependent stages of B cell development and waned upon entry into the small Pre-B cell stage.
309 These findings demonstrate that Let-7 dependent and independent targets of the LIN28B
310 molecular program alternates along the B cell differentiation axis. We propose that the LIN28B
311 induced increase in ribosomal protein levels may cooperate with its effects on c-MYC
312 expression to elevate global protein synthesis during the later stages of bone marrow B cell
313 development.
314
315 IL-7 is a major trophic factor driving c-MYC expression prior to the Pre-BCR checkpoint (2,
316 40). We therefore hypothesized that its potent effects on Pro-B cells might mask any LIN28B
317 mediated c-MYC up-regulation. To test this, we expanded B cell precursors from control and
318 tet-LIN28B bone marrow under saturating IL-7 conditions for five days, before replating the
319 cells under limiting doses of IL-7 (Figure 3D) (Mandal 2019). As expected, IL-7 withdrawal
320 led to a drastic decrease in c-MYC and a collapse in protein synthesis of Pro-B cells (Figure
321 3E-F). This decrease in c-MYC protein was substantially cushioned by tet-LIN28B (Figure 3E
322 left). The same trend was also observed for protein synthesis (Figure 3E right), although it was
323 not statistically significant (Figure 3F right). Consistent with the lack of IL-7Ra expression in
324 Imm-B cells, no effect of IL-7 titration was observed (Figure 3G). Taken together, we
325 demonstrate that LIN28B exerts an effect on the MYC/ribosome axis and that this effect is
326 masked by IL-7 signaling during the Pro-B and large Pre-B cell stages. These findings provide
327 an explanation to the stage specific effects of LIN28B on the c-MYC/ribosome axis during B
328 cell development (Figure 3H).
329

330 **Neonatal B cell development relies on a heightened level of protein synthesis**

331 Endogenous LIN28B expression is developmentally limited to fetal and neonatal life. FACS
332 analysis of LIN28B-eGFP reporter mice (34) captured its window of expression in B cell
333 precursors as it gradually diminished to background levels after day 10 (Figure 4A). Following
334 the same kinetics, neonatal B cell development exhibits a transient elevation of protein
335 synthesis rates as measured by AHA uptake (Figure 4B). This effect was LIN28B dependent
336 during the small Pre-B and Imm-B cell stages and fully abolished in 3-day-old neonates that
337 lacked endogenous *Lin28b* (Figure 4C). In contrast, *Lin28b* deficiency does not ablate
338 increased protein synthesis in neonatal Pro-B cells. These findings establish increased protein
339 synthesis as a hallmark of early life B cell development and confirm our observations from tet-
340 LIN28B mice in the context of wildtype neonates.

341

342 To investigate the importance of protein synthesis for neonatal B cell development, we took
343 advantage of the ribosomal protein hypomorphic $Rpl24^{WT/Bst}$ (Bst) mouse model. This model
344 carries a mutation that disrupts *Rpl24* mRNA splicing and thereby ribosome biogenesis,
345 exhibiting a 30% reduction in overall protein synthesis (41). This reduction in protein synthesis
346 does not affect normal adult B lymphopoiesis (38), but is sufficient to impair Eμ-MYC driven
347 oncogenesis (42). Given our findings, we hypothesized that early-life B lymphopoiesis might
348 be more sensitive to minor constraints in protein synthesis. Indeed, our analysis show stunted
349 B cell development in Bst neonates (Figure 4D) caused by a collapse in cell numbers at the
350 large Pre-B cell stage and beyond. This phenotype was most severe in three-day-old neonates
351 but became fully resolved by postnatal day 19. Taken together, these findings demonstrate that
352 neonatal B lymphopoiesis is more sensitive to constraints in protein synthesis compared to the
353 adult and therefore exhibits signs of ribosome addiction.

354

355 **Elevated protein synthesis is required for the output of CD5+ B-1 cells early in life**

356 The early-life expression of *Lin28b* allows for the developmental progression of self-reactive
357 B cell precursors into the mature B cell pool, including the output of CD5+ B-1 cells (19, 20).
358 This relaxation in the central tolerance threshold is evident in recently selected Imm-B cells
359 where LIN28B expression increases surface levels of CD5, a marker for self-reactivity (19).
360 Interestingly, further analysis of Imm-B cells revealed that CD5 expression induced by LIN28B
361 positively correlated with protein synthesis levels (Figure 5A-B). Thus, enhanced protein
362 synthesis may be important for the developmental progression of self-reactive B cells destined
363 for the CD5+ B-1 fate. To test this, we treated LIN28B induced mice with a single dose of
364 intraperitoneally administered Rapamycin to acutely dampen protein synthesis (Figure 5C)
365 (43). As expected, the treatment yielded a moderate reduction in protein synthesis levels in
366 both control and tet-LIN28B Imm-B cells (Figure 5D). This treatment selectively diminished
367 the CD5 levels in tet-LIN28B induced Imm-B cells (Figure 5E-F) demonstrating that LIN28B
368 dependent output of self-reactive B cells depends on increased protein synthesis.

369

370 Finally, to investigate the effect of constrained protein synthesis on early life B cell output, we
371 measured the abundance of CD5+ B-1 cells in 19-day-old Bst mice. This timepoint was
372 selected to evaluate B-1 cell output with minimal influence by peripheral homeostatic
373 expansion. FACS analysis identified a significant decrease in the absolute number of peritoneal
374 cavity (PerC) CD5+ B-1 cells of Bst mice as compared to littermate controls (Figure 5G).
375 Further analysis of their reactivity against the predominant self-membrane component
376 phosphatidyl choline (PtC) demonstrated a three-fold decrease of PtC reactive CD5+ B-1 B
377 cells in Bst mice (Figure 5H-I). We therefore conclude that elevated protein synthesis is a
378 central distinguishing parameter in neonatal B lymphopoiesis that potentiates the output of
379 CD5+ B-1 cells with self-reactive BCR specificities.

380 **Discussion**

381 Our findings identify elevated protein synthesis as a hallmark of early life B cell development
382 that is required for the time restricted output of self-reactive B-1 cells during ontogeny. This is
383 mediated in part by the endogenous expression of the heterochronic RNA-binding protein
384 LIN28B. Its expression naturally wanes during the first weeks of life and ectopic LIN28B
385 expression is sufficient to recapitulate elevated protein synthesis in adult mice. Consistent with
386 previous reports, we show that LIN28B directly binds to ribosomal protein transcripts and
387 correlates with enhanced ribosomal protein expression in primary B cell precursors.
388 Interestingly, this phenotype is shared across all stages of B cell development and precedes the
389 increase in ribosomal biogenesis and protein synthesis first observed in small Pre-B cells. The
390 delayed effect on ribosomal function coincides with the appearance of LIN28B induced c-
391 MYC expression. Thus, increased ribosomal protein components was not sufficient to promote
392 ribosome biogenesis in the absence of elevated c-MYC expression. We propose that LIN28B
393 mediated post-transcriptional regulation of ribosomal proteins cooperates with the
394 transcriptional program of c-MYC to elevate protein synthesis during B cell development. The
395 precise extent and mechanism by which LIN28B superimposes post-transcriptional regulation
396 on the backdrop of a c-MYC induced transcriptome have not been disentangled in this study.
397 Nevertheless, our findings address a gap in the knowledge of neonatal B cell development with
398 important implications in neonatal adaptive immune responses.

399

400 Protein synthesis is the most energy consuming biosynthetic process in the cell and subject to
401 the constraints imposed by hundreds of components required for ribosome assembly (44).
402 Indeed, protein synthesis rates give an accurate account of the overall cellular metabolism (45).
403 And yet, its ability to control the development and function of immune cells that require rapid
404 expansion and contraction of cellular growth has been an under-explored subject of

405 investigation. Our results using AHA metabolic labelling to measure protein synthesis
406 confirmed dynamic changes in cellular metabolism that underly proliferative bursts following
407 successful BCR checkpoints (1). Importantly, we demonstrate the ability of LIN28B to cushion
408 the biggest drop in protein synthesis in the small Pre-B cell stage. Interestingly, the restricted
409 metabolism of small Pre-B cells has been implicated as a mechanism to safeguard the central
410 tolerance checkpoint through enforcing nutrient stress and negative selection upon strong BCR
411 engagement (5). This notion is highly compatible with our observation that LIN28B promotes
412 protein synthesis to augment positive selection and the output of self-reactive CD5+ B-1 cells
413 early in life. Thus, we propose that the relatively mild increase in protein synthesis by LIN28B
414 provides sufficient relaxation of the metabolic constraints during B cell maturation, to
415 qualitatively shift the neonatal BCR repertoire.
416
417 In Pro-B cells, IL-7 signaling and downstream mTORC1 activation is the principal driver of c-
418 MYC expression and acts to promote biomass accumulation and proliferation (Zeng et al
419 2018). The attenuation of IL-7 signaling during B cell development marks a dramatic decrease
420 in overall bioenergetic state whereby preBCR/BCR mediated signals become dominant in cell
421 fate instruction. Interestingly, this metabolic gear shift correlates with distinct outcomes of
422 LIN28B mediated effects. While de-repression of Let-7 targets is most prominent during the
423 IL-7 dependent stages, the opposite is true of its effect on protein synthesis which appear later.
424 This could be due to changes in the abundance of LIN28B/Let-7 RNA substrates in
425 proliferating versus quiescent cells respectively. Therefore, our findings implicate metabolic
426 status as a powerful rheostat of LIN28B action.
427
428 In neonatal B cell development, protein synthesis is higher during all stages compared to the
429 adult. However, LIN28B is neither necessary nor sufficient to account for the observed effect

430 in Pro-B cells under IL-7 sufficient conditions, suggesting that other developmentally restricted
431 neonatal factors are at play. To this end, LIN28B has previously been shown to act in an
432 autoregulatory loop with Igf2bp3, another RNA-binding protein which binds a substantially
433 overlapping transcript pool to promote a fetal-like lymphopoiesis (26). It is therefore possible
434 that partial redundancy with Igf2bp3 could account for certain LIN28B independent effects of
435 early life B cell development. In the context of IL-7 deprivation however, Pro-B cells become
436 rapidly sensitized to LIN28B mediated effects. This finding is consistent with the previously
437 reported ability of LIN28B to circumvent the strict requirement for IL-7Ra during adult B
438 lymphopoiesis (16). Thus, overlapping effects by both LIN28B and IL-7 on the very same c-
439 MYC/ribosome axis may offer an explanation to the decreased reliance on IL-7 for early life
440 B lymphopoiesis (6).
441
442 In this study, we have not resolved the fates of LIN28B bound transcripts in the rapidly
443 alternating stages of B cell development. One obstacle preventing the examination of the
444 context dependent effects of LIN28B is the limited cellular material from quiescent cell types
445 *in vivo.* Methods such as polysome sequencing to profile changes in protein translation are
446 optimized for proliferating cells. However, our findings make clear that *in vitro* culturing or
447 oncogene mediated transformation will not recapitulate LIN28B mediated effects in small Pre-
448 B cells. Thus, the prohibitive nature of quiescent cells poses technical challenges that must be
449 overcome to address the context dependent actions of LIN28B *in vivo*. Nevertheless, our results
450 demonstrate that protein synthesis is an important differentially regulated feature of neonatal
451 B lymphopoiesis and open new avenues for future investigations. In the context of B cell
452 neoplasms, protein synthesis is a key mediator of c-MYC driven oncogenesis (42). Considering
453 the strong infant and childhood association of B cell precursor acute lymphoblastic leukemia
454 incidence, it will be important to investigate a potential role for increased ribosome addiction

455 in the pathogenesis of the disease. In the context of the neonatal B cell responses, we and others
456 have demonstrated that neonatal immunization produces unique B cell memory clones not
457 generated by adult mice immunized with the same antigen (46, 47). Our current findings that
458 enhanced protein synthesis critically shapes the output of naïve B cell specificities implicates
459 ribosomal control in the formation of a layered immune system. Going forward, the extent to
460 which this may instruct early life B cell memory formation remains an outstanding question of
461 great interest.

Acknowledgements

We thank Jonas Ungerbäck and Johanna Tingvall-Gustafsson for help with bioinformatics. We thank Jenny Hansson, Leal Oburoglu, and Svetlana Soboleva for their input. Finally, we also thank the FACS and Bioinformatics core facilities at the Lund Stem Cell Center for their support.

Footnotes

Funding

J.Y. was supported by the Swedish Research Council, the Swedish Cancer Society, the European Research Council (715313), Knut and Alice Wallenberg Foundation and the Wenner-Gren Foundations.

472 **Figure Legends**

473

474 **Figure 1. LIN28B binds to ribosomal protein transcripts in primary B cell precursors**

475

476 **(A)** Schematic of experimental setup for the identification of LIN28B-mRNA targets. B cell
477 progenitors were expanded from whole, adult bone marrow in the presence of IL-7 (20 ng/mL)
478 and Dox (0.1 µg/mL) for five days prior to RNA-IP. Co-immunoprecipitated mRNA from two
479 tet-LIN28B and one control mouse were individually subjected to RNA-seq. **(B)** Scatter plot
480 showing enrichment correlation between the two tet-LIN28B samples. LIN28B IP/input
481 enrichment ratio of least two-fold (n=238) were used for subsequent analyses. **(C)** Average
482 enrichment ranking of the tet-LIN28B samples compared to the control sample. **(D)** Gene
483 ontology analysis of enriched transcripts. **(E)** Analysis of overlapping genes between our RIP-
484 targets and previously published LIN28B-mRNA interactome data (22, 31). **(F)** Plot showing
485 how gene ontology terms identified in D compares and overlaps with LIN28B interacting
486 transcripts identified in the indicated studies.

487

488 **Figure 2. LIN28B enhances ribosome biogenesis and protein synthesis in small Pre-B and**
489 **Imm-B cells**

490

491 **(A)** Representative western blot analysis for indicated ribosomal proteins on 50,000 FACS
492 sorted B cell progenitors from tet-LIN28B or littermate control mice following 10 days of Dox
493 induction. Representative of at least two biological replicates per cell type and genotype. Blots
494 were cropped to improve clarity. **(B)** qRT-PCR of 18S rRNA and **C)** 45S pre-rRNA from
495 50,000 FACS sorted B cell progenitors, expression values were normalized relative to the
496 littermate control Imm-B cells. Data from 4-5 biological replicates and 2 experimental

497 replicates. **(D)** Representative FACS histogram overlays of L-Azidohomoalanine (AHA)
498 uptake, corresponding to their protein synthesis rates, in the indicated progenitor subsets. **(E)**
499 Average of the median fluorescence intensity (MFI) for AHA, as shown in D. Data from 7
500 biological replicates and 3 experimental replicates. **(F)** Average AHA MFI from FACS analysis
501 on peritoneal cavity (PerC) B cell subsets. Data from 3-4 biological replicates and 2
502 experimental replicates. Wilcox test was used to calculate p-values. *p<0.05, **p<0.01,
503 ***p<0.001. Bars show the mean and error bars show standard deviation.
504
505 **Figure 3. IL-7 dependent stimulation of the c-MYC/ribosome axis masks the anabolic**
506 **effects of LIN28B in Pro-B cells**
507
508 **(A)** Representative histograms showing intracellular FACS analysis of c-MYC protein
509 expression. **(B) c-**MYC median fluorescence intensity (MFI) levels in B cell precursors, from
510 the indicated genotypes following 10 days of doxycycline induction. Data is represented as
511 average values normalized per cell type to the littermate control. Data from 7-12 biological
512 replicates and 6 experimental replicates. **(C)** Gene set enrichment analysis (GSEA) of RNA-
513 seq data from FACS sorted B cell precursors for the indicated signatures (right Y axis) and cell
514 types. LIN28B enrichment rank was Wald's stat from DESeq2, comparing each cell type for
515 differentially expressed genes in tet-LIN28B to control mice. The Pro-B cells were sorted on
516 high FSC-A, in addition to the immunophenotype as stated under Materials and Methods. Data
517 from 3-6 biological replicates. **(D)** Experimental setup for measuring the impact of IL-7
518 withdrawal on LIN28B mediated effects on c-MYC protein expression and L-
519 azidohomoalanine (AHA) uptake in cKit+ Pro-B cells. **(E)** Representative FACS histograms
520 for the indicated IL-7 conditions, showing the measured c-MYC protein expression (left) and
521 AHA uptake (right). **(F)** Average MFI of c-MYC expression and AHA uptake FACS in Pro-B

522 cells kept under indicated IL-7 conditions. Values were normalized to littermate controls at
523 max IL-7 concentrations 20 ng/mL. Data from three separate experiments, with 3-4 littermate
524 and Lin28b mice depending on cell type. **(G)** Same as in (F), but for IgM+ Imm-B cells. **(H)**
525 Schematic illustration of the proposed LIN28B mechanism in B cell precursors. Wilcox test
526 was used to calculate p-values in B. T-test was used to calculate p-values in F and G. *p<0.05,
527 **p<0.01, ***p<0.001. Bars show the mean and error bars show standard deviation.
528

529 **Figure 4. Neonatal B cell development is dependent on enhanced protein synthesis**

530 **(A)** Average frequency of *Lin28b*-eGFP positivity of the indicated B cell precursor subsets,
531 from *Lin28b*-eGFP mice at the indicated age. 4-10 biological replicates, over the different days
532 of analysis. **(B)** Average AHA MFI normalized to adult samples. Three biological replicates
533 each, two separate experiments. **(C)** Average AHA MFI from 3-day old *Lin28b* WT (n=5) or
534 KO (n=5) neonates normalized to WT adult samples. Data from two separate experiments. **(D)**
535 Average frequency of B cell precursors from neonatal or adult Rpl24-Bst heterozygous mutants
536 or littermate control mice, at the indicated ages. Data from at least two separate experiments,
537 number of mice is indicated in figure legends. T-test was used to calculate p-values in B, C,
538 and D. *p<0.05, **p<0.01, ***p<0.001. Bars show the mean and error bars show standard
539 deviation.
540

541 **Figure 5. Elevated protein synthesis is required for the output of CD5+ B-1 cells early in**
542 **life**

543 **(A)** (Left) Representative FACS plots for CD5 expression in Imm-B cells from the indicated
544 genotypes treated with doxycycline for 10 days. (Right) Histogram showing the L-
545 azidohomoalanine (AHA) uptake of the individual CD5 slices. **(B)** Average AHA median
546 fluorescence intensity (MFI) within individual CD5 slices shown as relative values to control

547 Imm-B cells (n=4-5). Data from four separate experiments. **(C)** Schematic for Rapamycin
548 (Rapa, 2 mg/kg) treatment of tet-LIN28B and littermate control mice with Rapamycin, or
549 vehicle control treatment (EtOH). Mice were treated by a single, intra-peritoneal injection and
550 analyzed 24hrs later. **(D)** AHA MFI from Imm-B cells of the indicated genotype and treatment,
551 shown relative to EtOH treated littermate controls (n=5-6). Data from four separate
552 experiments. **(E)** Representative FACS histograms showing CD5 levels. **(F)** Average CD5 MFI
553 from Imm-B cells of the indicated genotypes and treatment, shown relative to EtOH treated
554 littermate controls (n=4-7). **(G)** Absolute number of peritoneal cavity (PerC) CD5+ B-1 cells
555 in day 19 neonates of the indicated genotypes (n=4). **(H)** Representative FACS plots showing
556 the frequency of CD5+ PtC reactive B cells from 19-day old neonates of the indicated
557 genotypes. **(I)** Average frequency of CD5+PtC+ B cells in day 19 neonates of the indicated
558 genotypes (n=4). Wilcox test was used to calculate p-values *$p<0.05$, **$p<0.01$. Bars show the
559 mean and error bars show standard deviation.

560 **References**

561 1. Clark, M. R., M. Mandal, K. Ochiai, and H. Singh. 2014. Orchestrating B cell lymphopoiesis
562 through interplay of IL-7 receptor and pre-B cell receptor signalling. *Nat Rev Immunol* 14: 69-
563 80.
564 2. Zeng, H., M. Yu, H. Tan, Y. Li, W. Su, H. Shi, Y. Dhungana, C. Guy, G. Neale, C. Cloer, J. Peng,
565 D. Wang, and H. Chi. 2018. Discrete roles and bifurcation of PTEN signaling and mTORC1-
566 mediated anabolic metabolism underlie IL-7-driven B lymphopoiesis. *Sci Adv* 4: eaar5701.
567 3. Mandal, M., M. K. Okoreeh, D. E. Kennedy, M. Maienschein-Cline, J. Ai, K. C. McLean, N.
568 Kaverina, M. Veselits, I. Aifantis, F. Gounari, and M. R. Clark. 2019. CXCR4 signaling directs
569 Igk recombination and the molecular mechanisms of late B lymphopoiesis. *Nat Immunol* 20:
570 1393-1403.
571 4. Nemazee, D. 2017. Mechanisms of central tolerance for B cells. *Nat Rev Immunol* 17: 281-
572 294.
573 5. Muschen, M. 2019. Metabolic gatekeepers to safeguard against autoimmunity and
574 oncogenic B cell transformation. *Nat Rev Immunol* 19: 337-348.
575 6. Kikuchi, K., and M. Kondo. 2006. Developmental switch of mouse hematopoietic stem cells
576 from fetal to adult type occurs in bone marrow after birth. *Proc Natl Acad Sci U S A* 103:
577 17852-17857.
578 7. Hayakawa, K., M. Asano, S. A. Shinton, M. Gui, D. Allman, C. L. Stewart, J. Silver, and R. R.
579 Hardy. 1999. Positive selection of natural autoreactive B cells. *Science* 285: 113-116.
580 8. Chen, J. W., T. A. Rice, J. M. Bannock, A. A. Bielecka, J. D. Strauss, J. R. Catanzaro, H. Wang, L.
581 C. Menard, J. H. Anolik, N. W. Palm, and E. Meffre. 2020. Autoreactivity in naive human fetal
582 B cells is associated with commensal bacteria recognition. *Science* 369: 320-325.
583 9. Wong, J. B., S. L. Hewitt, L. M. Heltemes-Harris, M. Mandal, K. Johnson, K. Rajewsky, S. B.
584 Koralov, M. R. Clark, M. A. Farrar, and J. A. Skok. 2019. B-1a cells acquire their unique
585 characteristics by bypassing the pre-BCR selection stage. *Nat Commun* 10: 4768.
586 10. Baumgarth, N. 2011. The double life of a B-1 cell: self-reactivity selects for protective
587 effector functions. *Nat Rev Immunol* 11: 34-46.
588 11. Ambros, V., and H. R. Horvitz. 1984. Heterochronic mutants of the nematode Caenorhabditis
589 elegans. *Science* 226: 409-416.
590 12. Copley, M. R., and C. J. Eaves. 2013. Developmental changes in hematopoietic stem cell
591 properties. *Exp Mol Med* 45: e55.
592 13. Zhou, Y., Y. S. Li, S. R. Bandi, L. Tang, S. A. Shinton, K. Hayakawa, and R. R. Hardy. 2015.
593 Lin28b promotes fetal B lymphopoiesis through the transcription factor Arid3a. *J Exp Med*
594 212: 569-580.
595 14. Copley, M. R., S. Babovic, C. Benz, D. J. Knapp, P. A. Beer, D. G. Kent, S. Wohrer, D. Q.
596 Treloar, C. Day, K. Rowe, H. Mader, F. Kuchenbauer, R. K. Humphries, and C. J. Eaves. 2013.
597 The Lin28b-let-7-Hmga2 axis determines the higher self-renewal potential of fetal
598 haematopoietic stem cells. *Nat Cell Biol* 15: 916-925.
599 15. Sampson, V. B., N. H. Rong, J. Han, Q. Yang, V. Aris, P. Soteropoulos, N. J. Petrelli, S. P. Dunn,
600 and L. J. Krueger. 2007. MicroRNA let-7a down-regulates MYC and reverts MYC-induced
601 growth in Burkitt lymphoma cells. *Cancer Res* 67: 9762-9770.
602 16. Yuan, J., C. K. Nguyen, X. Liu, C. Kanellopoulou, and S. A. Muljo. 2012. Lin28b reprograms
603 adult bone marrow hematopoietic progenitors to mediate fetal-like lymphopoiesis. *Science*
604 335: 1195-1200.
605 17. Kristiansen, T. A., E. Jaensson Gyllenback, A. Zriwil, T. Bjorklund, J. A. Daniel, E. Sitnicka, S.
606 Soneji, D. Bryder, and J. Yuan. 2016. Cellular Barcoding Links B-1a B Cell Potential to a Fetal
607 Hematopoietic Stem Cell State at the Single-Cell Level. *Immunity* 45: 346-357.
608 18. Wang, J., E. M. Wissink, N. B. Watson, N. L. Smith, A. Grimson, and B. D. Rudd. 2016. Fetal
609 and adult progenitors give rise to unique populations of CD8+ T cells. *Blood* 128: 3073-3082.

610 19. Vanhee, S., H. Akerstrand, T. A. Kristiansen, S. Datta, G. Montano, S. Vergani, S. Lang, J.
611 Ungerback, A. Doyle, K. Olsson, G. Beneventi, C. T. Jensen, C. Bellodi, S. Soneji, M.
612 Sigvardsson, E. J. Gyllenback, and J. Yuan. 2019. Lin28b controls a neonatal to adult switch in
613 B cell positive selection. *Sci Immunol* 4.
614 20. Xu, X., M. Deobagkar-Lele, K. R. Bull, T. L. Crockford, A. J. Mead, A. P. Cribbs, D. Sims, C.
615 Anzilotti, and R. J. Cornall. 2020. An ontogenetic switch drives the positive and negative
616 selection of B cells. *Proc Natl Acad Sci U S A* 117: 3718-3727.
617 21. Benhamou, D., V. Labi, R. Novak, I. Dai, S. Shafir-Alon, A. Weiss, R. Gaujoux, R. Arnold, S. S.
618 Shen-Orr, K. Rajewsky, and D. Melamed. 2016. A c-Myc/miR17-92/Pten Axis Controls PI3K-
619 Mediated Positive and Negative Selection in B Cell Development and Reconstitutes CD19
620 Deficiency. *Cell Rep* 16: 419-431.
621 22. Graf, R., M. Munschauer, G. Mastrobuoni, F. Mayr, U. Heinemann, S. Kempa, N. Rajewsky,
622 and M. Landthaler. 2013. Identification of LIN28B-bound mRNAs reveals features of target
623 recognition and regulation. *RNA Biol* 10: 1146-1159.
624 23. Wilbert, M. L., S. C. Huelga, K. Kapeli, T. J. Stark, T. Y. Liang, S. X. Chen, B. Y. Yan, J. L.
625 Nathanson, K. R. Hutt, M. T. Lovci, H. Kazan, A. Q. Vu, K. B. Massirer, Q. Morris, S. Hoon, and
626 G. W. Yeo. 2012. LIN28 binds messenger RNAs at GGAGA motifs and regulates splicing factor
627 abundance. *Mol Cell* 48: 195-206.
628 24. Cho, J., H. Chang, S. C. Kwon, B. Kim, Y. Kim, J. Choe, M. Ha, Y. K. Kim, and V. N. Kim. 2012.
629 LIN28A is a suppressor of ER-associated translation in embryonic stem cells. *Cell* 151: 765-
630 777.
631 25. Hafner, M., K. E. Max, P. Bandaru, P. Morozov, S. Gerstberger, M. Brown, H. Molina, and T.
632 Tuschl. 2013. Identification of mRNAs bound and regulated by human LIN28 proteins and
633 molecular requirements for RNA recognition. *RNA* 19: 613-626.
634 26. Wang, S., B. Chim, Y. Su, P. Khil, M. Wong, X. Wang, A. Foroushani, P. T. Smith, X. Liu, R. Li, S.
635 Ganesan, C. Kanellopoulou, M. Hafner, and S. A. Muljo. 2019. Enhancement of LIN28B-
636 induced hematopoietic reprogramming by IGF2BP3. *Genes Dev* 33: 1048-1068.
637 27. Basak, A., M. Munschauer, C. A. Lareau, K. E. Montbleau, J. C. Ulirsch, C. R. Hartigan, M.
638 Schenone, J. Lian, Y. Wang, Y. Huang, X. Wu, L. Gehrke, C. M. Rice, X. An, H. A. Christou, N.
639 Mohandas, S. A. Carr, J. J. Chen, S. H. Orkin, E. S. Lander, and V. G. Sankaran. 2020. Control
640 of human hemoglobin switching by LIN28B-mediated regulation of BCL11A translation. *Nat*
641 *Genet* 52: 138-145.
642 28. Osborne, J. K., M. A. Kinney, A. Han, K. E. Akinnola, A. V. Yermalovich, L. T. Vo, D. S. Pearson,
643 P. M. Sousa, S. Ratanasirintrawoot, K. M. Tsanov, J. Barragan, T. E. North, R. J. Metzger, and
644 G. Q. Daley. 2021. Lin28 paralogs regulate lung branching morphogenesis. *Cell Rep* 36:
645 109408.
646 29. Madison, B. B., Q. Liu, X. Zhong, C. M. Hahn, N. Lin, M. J. Emmett, B. Z. Stanger, J. S. Lee, and
647 A. K. Rustgi. 2013. LIN28B promotes growth and tumorigenesis of the intestinal epithelium
648 via Let-7. *Genes Dev* 27: 2233-2245.
649 30. Tan, F. E., S. Sathe, E. C. Wheeler, and G. W. Yeo. 2021. Non-microRNA binding competitively
650 inhibits LIN28 regulation. *Cell Rep* 36: 109517.
651 31. Missios, P., E. L. da Rocha, D. S. Pearson, J. Philipp, M. M. Aleman, M. Pirouz, D. Farache, J.
652 W. Franses, C. Kubaczka, K. M. Tsanov, D. K. Jha, B. Pepe-Mooney, J. T. Powers, R. I. Gregory,
653 A. S. Lee, D. Dominguez, D. T. Ting, and G. Q. Daley. 2021. LIN28B alters ribosomal dynamics
654 to promote metastasis in MYCN-driven malignancy. *J Clin Invest* 131.
655 32. Peng, S., L. L. Chen, X. X. Lei, L. Yang, H. Lin, G. G. Carmichael, and Y. Huang. 2011. Genome-
656 wide studies reveal that Lin28 enhances the translation of genes important for growth and
657 survival of human embryonic stem cells. *Stem Cells* 29: 496-504.
658 33. Zhu, H., N. Shyh-Chang, A. V. Segre, G. Shinoda, S. P. Shah, W. S. Einhorn, A. Takeuchi, J. M.
659 Engreitz, J. P. Hagan, M. G. Kharas, A. Urbach, J. E. Thornton, R. Triboulet, R. I. Gregory, D.

660 Consortium, M. Investigators, D. Altshuler, and G. Q. Daley. 2011. The Lin28/let-7 axis
661 regulates glucose metabolism. *Cell* 147: 81-94.
662 34. Kristiansen, T. A., Q. Zhang, S. Vergani, E. Boldrin, N. Krausse, O. Andre, P. Nordenfelt, M.
663 Sigvardsson, D. Bryder, J. Ungerback, and J. Yuan. 2022. Developmental cues license
664 megakaryocyte priming in murine hematopoietic stem cells. *Blood Adv*.
665 35. Holl, T. M., B. F. Haynes, and G. Kelsoe. 2010. Stromal cell independent B cell development
666 in vitro: generation and recovery of autoreactive clones. *J Immunol Methods* 354: 53-67.
667 36. Ersching, J., A. Efeyan, L. Mesin, J. T. Jacobsen, G. Pasqual, B. C. Grabiner, D. Dominguez-
668 Sola, D. M. Sabatini, and G. D. Victora. 2017. Germinal Center Selection and Affinity
669 Maturation Require Dynamic Regulation of mTORC1 Kinase. *Immunity* 46: 1045-1058 e1046.
670 37. Shyh-Chang, N., H. Zhu, T. Yvanka de Soysa, G. Shinoda, M. T. Seligson, K. M. Tsanov, L.
671 Nguyen, J. M. Asara, L. C. Cantley, and G. Q. Daley. 2013. Lin28 enhances tissue repair by
672 reprogramming cellular metabolism. *Cell* 155: 778-792.
673 38. Signer, R. A., J. A. Magee, A. Salic, and S. J. Morrison. 2014. Haematopoietic stem cells
674 require a highly regulated protein synthesis rate. *Nature* 509: 49-54.
675 39. Ruggero, D. 2009. The role of Myc-induced protein synthesis in cancer. *Cancer Res* 69: 8839-
676 8843.
677 40. Morrow, M. A., G. Lee, S. Gillis, G. D. Yancopoulos, and F. W. Alt. 1992. Interleukin-7 induces
678 N-myc and c-myc expression in normal precursor B lymphocytes. *Genes Dev* 6: 61-70.
679 41. Oliver, E. R., T. L. Saunders, S. A. Tarle, and T. Glaser. 2004. Ribosomal protein L24 defect in
680 belly spot and tail (Bst), a mouse Minute. *Development* 131: 3907-3920.
681 42. Barna, M., A. Pusic, O. Zollo, M. Costa, N. Kondrashov, E. Rego, P. H. Rao, and D. Ruggero.
682 2008. Suppression of Myc oncogenic activity by ribosomal protein haploinsufficiency. *Nature*
683 456: 971-975.
684 43. Beretta, L., A. C. Gingras, Y. V. Svitkin, M. N. Hall, and N. Sonenberg. 1996. Rapamycin blocks
685 the phosphorylation of 4E-BP1 and inhibits cap-dependent initiation of translation. *EMBO J*
686 15: 658-664.
687 44. Buttgereit, F., and M. D. Brand. 1995. A hierarchy of ATP-consuming processes in
688 mammalian cells. *Biochem J* 312 (Pt 1): 163-167.
689 45. Arguello, R. J., A. J. Combes, R. Char, J. P. Gigan, A. I. Baaziz, E. Bousiquot, V. Camosseto, B.
690 Samad, J. Tsui, P. Yan, S. Boissonneau, D. Figarella-Branger, E. Gatti, E. Tabouret, M. F.
691 Krummel, and P. Pierre. 2020. SCENITH: A Flow Cytometry-Based Method to Functionally
692 Profile Energy Metabolism with Single-Cell Resolution. *Cell Metab* 32: 1063-1075 e1067.
693 46. Vergani, S., K. G. Muleta, C. Da Silva, A. Doyle, T. A. Kristiansen, S. Sodini, N. Krausse, G.
694 Montano, K. Kotarsky, J. Nakawesi, H. Akerstrand, S. Vanhee, S. L. Gupta, D. Bryder, W. W.
695 Agace, K. Lahl, and J. Yuan. 2022. A self-sustaining layer of early-life-origin B cells drives
696 steady-state IgA responses in the adult gut. *Immunity*.
697 47. New, J. S., B. L. P. Dizon, C. F. Fucile, A. F. Rosenberg, J. F. Kearney, and R. G. King. 2020.
698 Neonatal Exposure to Commensal-Bacteria-Derived Antigens Directs Polysaccharide-Specific
699 B-1 B Cell Repertoire Development. *Immunity* 53: 172-186 e176.

700

Figure 1

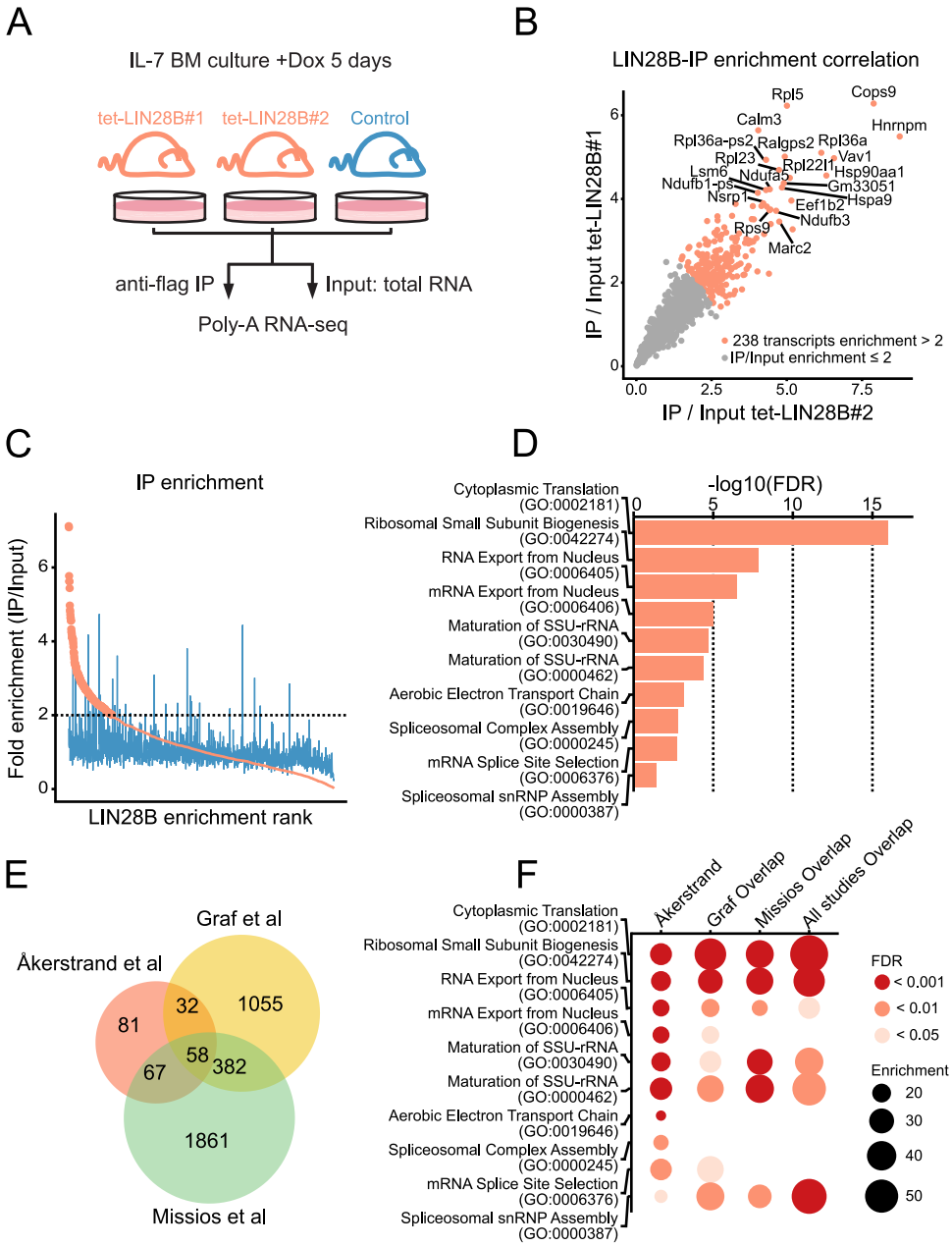
A
IL-7 BM culture +Dox 5 days
tet-LIN28B#1
tet-LIN28B#2
Control
anti-flag IP
Input: total RNA
Poly-A RNA-seq
B
LIN28B-IP enrichment correlation
IP / Input tet-LIN28B#1
IP / Input tet-LIN28B#2
238 transcripts enrichment > 2
IP/Input enrichment ≤ 2
Rpl5
Cops9
Calm3
Hnrnpm
Rpl36a-ps2
Ralgps2
Rpl36a
Rpl23
Vav1
Rpl22l1
Lsm6
Ndufa5
Hsp90aa1
Ndufb1-ps
Gm33051
Nsrp1
Hspa9
Eef1b2
Ndufb3
Rps9
Marc2
C
IP enrichment
Fold enrichment (IP/Input)
LIN28B enrichment rank
D
-log10(FDR)
Cytoplasmic Translation (GO:0002181)
Ribosomal Small Subunit Biogenesis (GO:0042274)
RNA Export from Nucleus (GO:0006405)
mRNA Export from Nucleus (GO:0006406)
Maturation of SSU-rRNA (GO:0030490)
Maturation of SSU-rRNA (GO:0000462)
Aerobic Electron Transport Chain (GO:0019646)
Spliceosomal Complex Assembly (GO:0000245)
mRNA Splice Site Selection (GO:0006376)
Spliceosomal snRNP Assembly (GO:0000387)
E
Graf et al
Åkerstrand et al
Missios et al
81
32
1055
58
67
382
1861
F
Åkerstrand
Graf Overlap
Missios Overlap
All studies Overlap
FDR
< 0.001
< 0.01
< 0.05
Enrichment
20
30
40
50

Figure 2

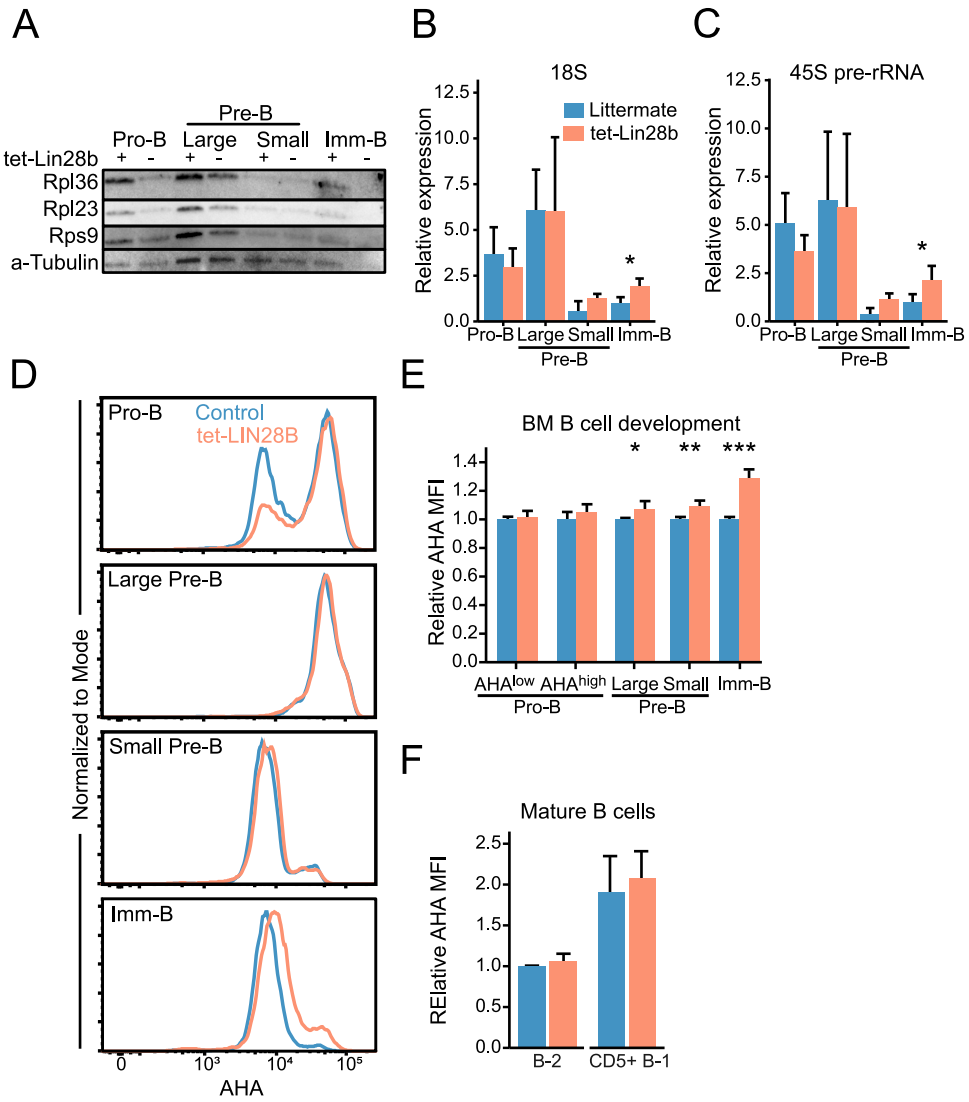
A
Pre-B
Pro-B
Large
Small
Imm-B
tet-Lin28b
+ - + - + - + -
Rpl36
Rpl23
Rps9
a-Tubulin
B
18S
Littermate
tet-Lin28b
Relative expression
12.5
10.0
7.5
5.0
2.5
0.0
*
Pro-B Large Small Imm-B
Pre-B
C
45S pre-rRNA
Relative expression
12.5
10.0
7.5
5.0
2.5
0.0
*
Pro-B Large Small Imm-B
Pre-B
D
Pro-B
Control
tet-LIN28B
Large Pre-B
Small Pre-B
Imm-B
Normalized to Mode
0
10³
10⁴
10⁵
AHA
E
BM B cell development
Relative AHA MFI
1.4
1.2
1.0
0.8
0.6
0.4
0.2
0.0
*
**
***
AHAlow AHAhigh Large Small Imm-B
Pro-B
Pre-B
F
Mature B cells
RElative AHA MFI
2.5
2.0
1.5
1.0
0.5
0.0
B-2
CD5+ B-1

Figure 3

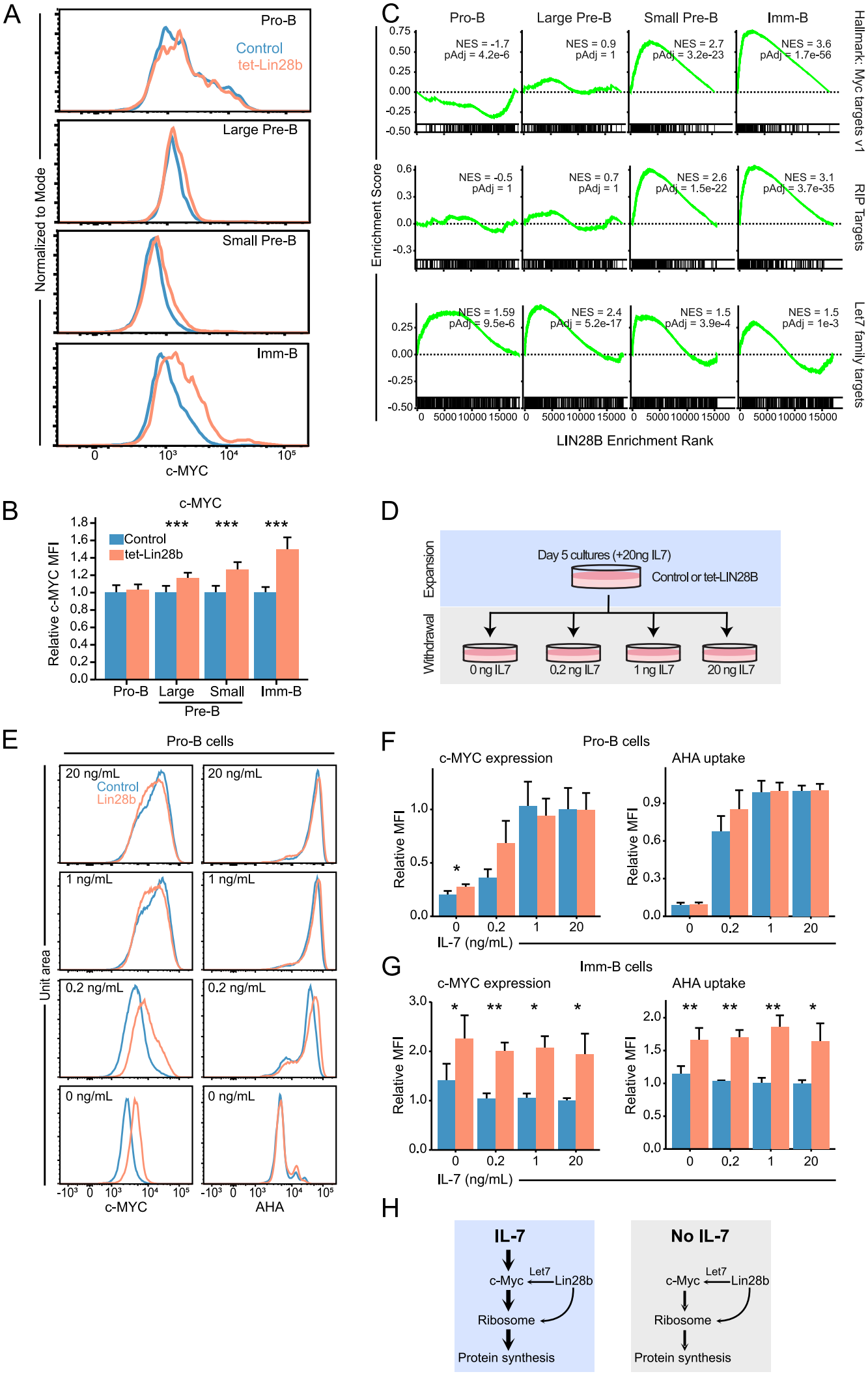
A
Pro-B
Control
tet-Lin28b
Large Pre-B
Small Pre-B
Imm-B
Normalized to Mode
c-MYC
B
c-MYC
Control
tet-Lin28b
Relative c-MYC MFI
Pro-B
Large
Small
Imm-B
Pre-B
C
Pro-B
Large Pre-B
Small Pre-B
Imm-B
NES = -1.7
pAdj = 4.2e-6
NES = 0.9
pAdj = 1
NES = 2.7
pAdj = 3.2e-23
NES = 3.6
pAdj = 1.7e-56
Hallmark: Myc targets v1
NES = -0.5
pAdj = 1
NES = 0.7
pAdj = 1
NES = 2.6
pAdj = 1.5e-22
NES = 3.1
pAdj = 3.7e-35
RIP Targets
NES = 1.59
pAdj = 9.5e-6
NES = 2.4
pAdj = 5.2e-17
NES = 1.5
pAdj = 3.9e-4
NES = 1.5
pAdj = 1e-3
Let7 family targets
Enrichment Score
LIN28B Enrichment Rank
D
Expansion
Day 5 cultures (+20ng IL7)
Control or tet-LIN28B
Withdrawal
0 ng IL7
0.2 ng IL7
1 ng IL7
20 ng IL7
E
Pro-B cells
20 ng/mL
Control
Lin28b
1 ng/mL
0.2 ng/mL
0 ng/mL
Unit area
c-MYC
AHA
F
Pro-B cells
c-MYC expression
AHA uptake
Relative MFI
IL-7 (ng/mL)
G
Imm-B cells
c-MYC expression
AHA uptake
Relative MFI
IL-7 (ng/mL)
H
IL-7
c-Myc
Let7
Lin28b
Ribosome
Protein synthesis
No IL-7
c-Myc
Let7
Lin28b
Ribosome
Protein synthesis

Figure 4

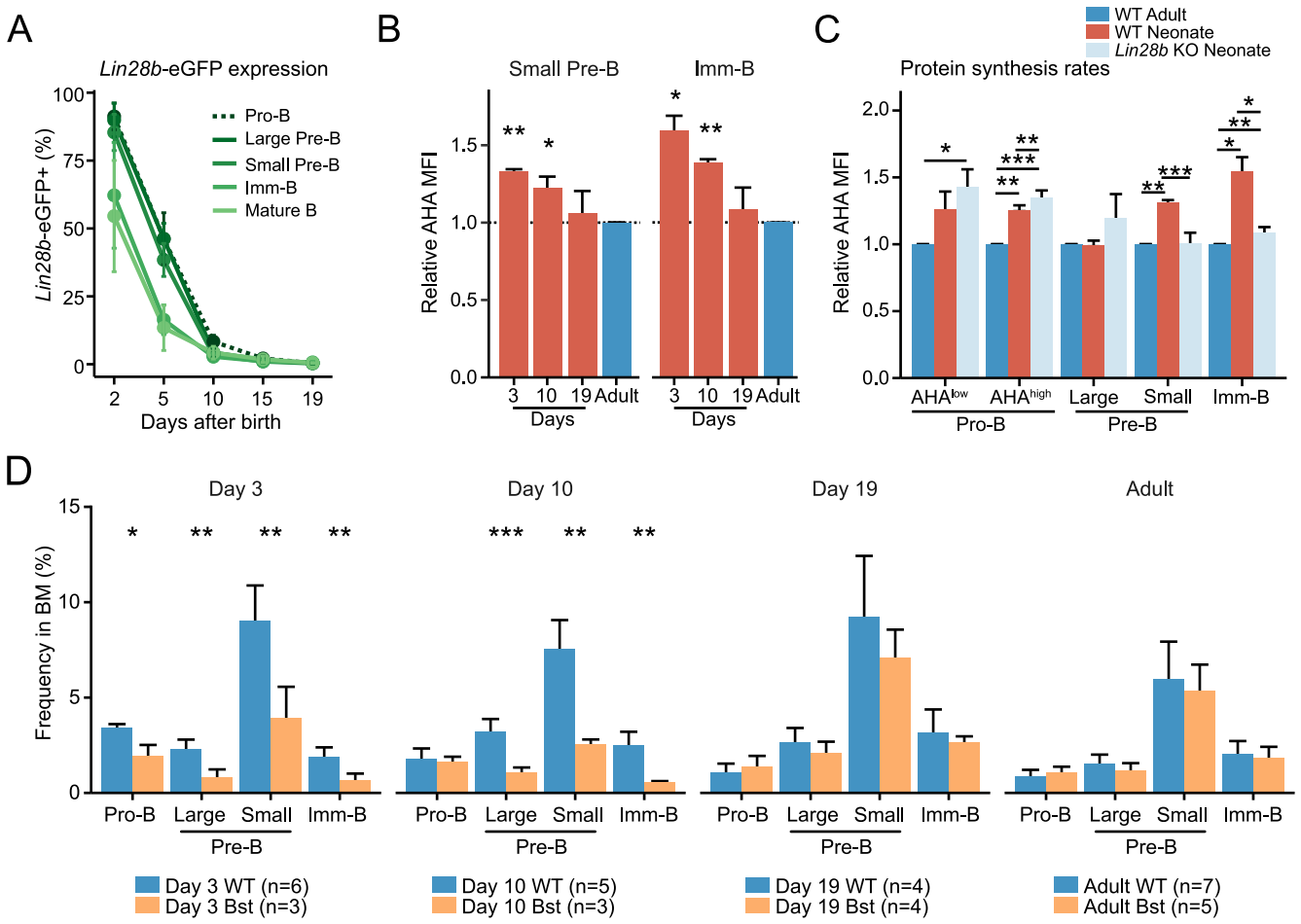
A
Lin28b-eGFP expression
Lin28b-eGFP+ (%)
Pro-B
Large Pre-B
Small Pre-B
Imm-B
Mature B
Days after birth
B
Small Pre-B
Imm-B
Relative AHA MFI
Days
C
WT Adult
WT Neonate
Lin28b KO Neonate
Protein synthesis rates
Relative AHA MFI
AHAlow
AHAhigh
Large
Small
Imm-B
Pro-B
Pre-B
D
Day 3
Day 10
Day 19
Adult
Frequency in BM (%)
Pro-B
Large
Small
Imm-B
Pre-B
Day 3 WT (n=6)
Day 3 Bst (n=3)
Day 10 WT (n=5)
Day 10 Bst (n=3)
Day 19 WT (n=4)
Day 19 Bst (n=4)
Adult WT (n=7)
Adult Bst (n=5)

Figure 5

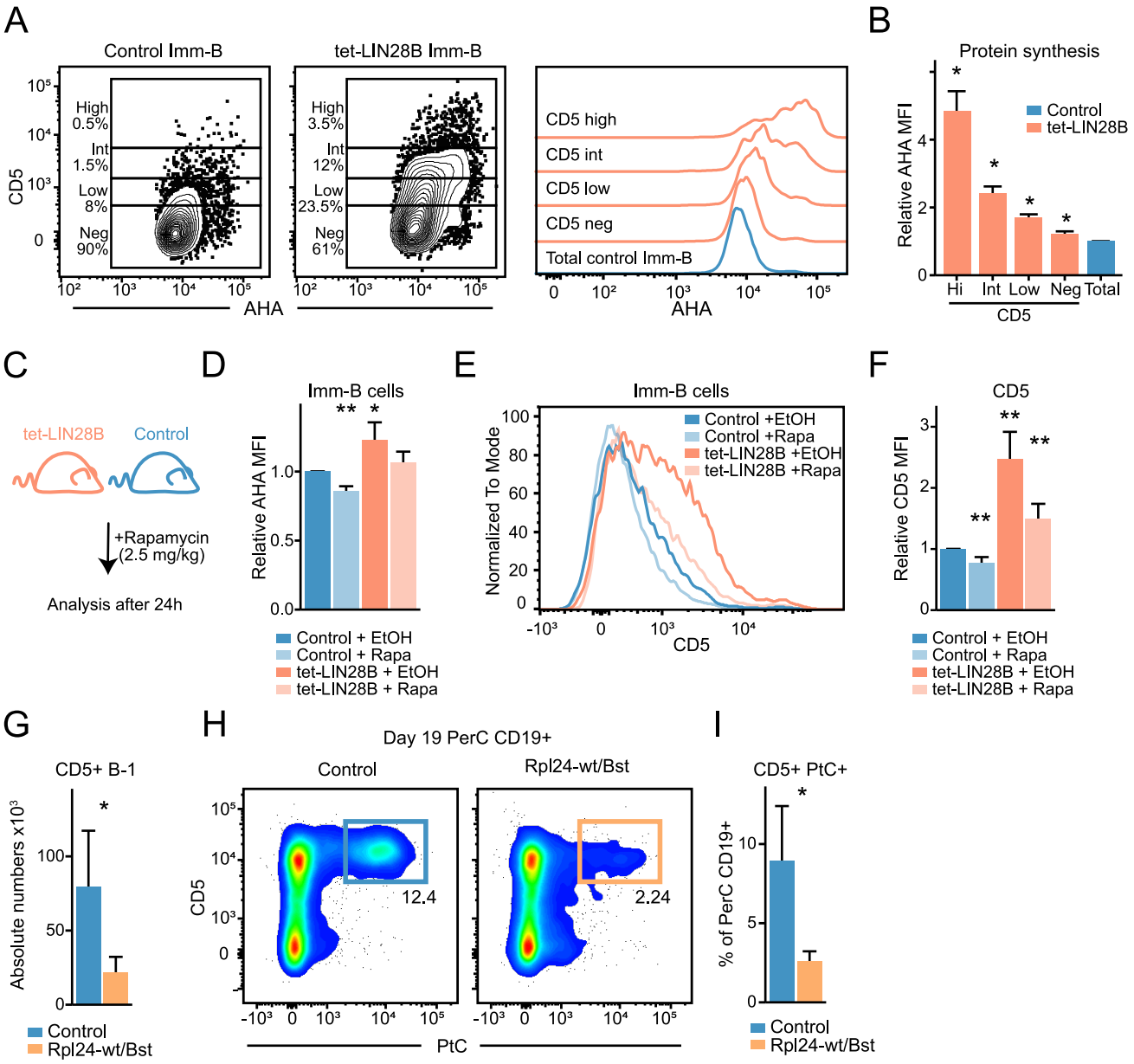
A
Control Imm-B
tet-LIN28B Imm-B
CD5
AHA
High 0.5%
Int 1.5%
Low 8%
Neg 90%
High 3.5%
Int 12%
Low 23.5%
Neg 61%
CD5 high
CD5 int
CD5 low
CD5 neg
Total control Imm-B
B
Protein synthesis
Relative AHA MFI
Control
tet-LIN28B
Hi
Int
Low
Neg
Total
CD5
C
tet-LIN28B
Control
+Rapamycin (2.5 mg/kg)
Analysis after 24h
D
Imm-B cells
Relative AHA MFI
Control + EtOH
Control + Rapa
tet-LIN28B + EtOH
tet-LIN28B + Rapa
E
Imm-B cells
Normalized To Mode
Control +EtOH
Control +Rapa
tet-LIN28B +EtOH
tet-LIN28B +Rapa
CD5
F
CD5
Relative CD5 MFI
Control + EtOH
Control + Rapa
tet-LIN28B + EtOH
tet-LIN28B + Rapa
G
CD5+ B-1
Absolute numbers x10³
Control
Rpl24-wt/Bst
H
Day 19 PerC CD19+
Control
Rpl24-wt/Bst
CD5
12.4
2.24
PtC
I
CD5+ PtC+
% of PerC CD19+
Control
Rpl24-wt/Bst